Si Nanoribbons on Ag(110) Studied by Grazing-Incidence X-Ray Diffraction, Scanning Tunneling Microscopy, and Density-Functional Theory: Evidence of a Pentamer Chain Structure

Geoffroy Prévot,[1,*] Conor Hogan,[2] Thomas Leoni,[3] Romain Bernard,[1] Eric Moyen,[3,‡] and Laurence Masson[3,†]
[1]Sorbonne Universités, UPMC Université Paris 06, CNRS-UMR 7588, Institut des NanoSciences de Paris, F-75005 Paris, France
[2]CNR-Istituto di Struttura della Materia, Via Fosso del Cavaliere 100, 00133 Rome, Italy and Dipartimento di Fisica, Università di Rome "Tor Vergata," Via della Ricerca Scientifica 1, 00133 Rome, Italy
[3]Aix Marseille Univ, CNRS, CINaM, Campus de Luminy, Case 913, 13288 Marseille Cedex 9, France
(Received 27 July 2016; revised manuscript received 10 October 2016; published 28 December 2016; publisher error corrected 12 January 2017)

We report a combined grazing incidence x-ray diffraction (GIXD), scanning tunneling microscopy (STM), and density-functional theory (DFT) study which clearly elucidates the atomic structure of the Si nanoribbons grown on the missing-row reconstructed Ag(110) surface. Our study allows us to discriminate between the theoretical models published in the literature, including the most stable atomic configurations and those based on a missing-row reconstructed Ag(110) surface. GIXD measurements unambiguously validate the pentamer model grown on the reconstructed surface, obtained from DFT. This pentamer atomistic model accurately matches the high-resolution STM images of the Si nanoribbons adsorbed on Ag(110). Our study closes the long-debated atomic structure of the Si nanoribbons grown on Ag(110) and definitively excludes a honeycomb structure similar to that of freestanding silicene.

DOI: 10.1103/PhysRevLett.117.276102

Since the prediction of metastable free-standing silicene [1,2], numerous experimental and theoretical studies have been devoted to epitaxial silicene, in particular on Ag surfaces [3]. Whereas Si forms two-dimensional (2D) silicene domains on Ag(111), with a buckled hexagonal structure [4,5], Si deposition at room temperature on Ag(110) leads to the synthesis of straight, long (up to several hundred nanometers), and defect-free one-dimensional (1D) nanostructures. These Si single nanoribbons (SNRs), with a width of 0.8 nm, are randomly distributed on silver terraces [6]. For Si deposition at 460 K, they self-assemble in (5×2) or $c(10 \times 2)$ unit cells to form a 1D grating composed of double nanoribbons (DNRs) with a width of 1.6 nm [7,8].

A long debate concerning the atomic structure of these nanoribbons (NRs) began after the reported graphenelike electronic signature measured by angle-resolved photoelectron spectroscopy (ARPES) and attributed to the silicene character of the Si NRs grown on Ag(110) [9]. Because of the high control over their width, such NRs may appear as an alternative to graphene NRs. They can also advantageously be used as a 1D template with a short- and long-range high structural order for the growth of Co chain nanomagnets [10]. Moreover, a strong resistance of the Si NRs towards oxidation has been reported using photoemission spectroscopy and low-energy electron diffraction [11]. The scope of potential applications of these unique Si-based 1D nanostructures with a high aspect ratio is wide [12]. In addition to the reported silicene nature of these nanostructures, the Si NRs could be used as building blocks to produce functional architectures upon, for instance, supramolecular or covalent assembly, aiming at molecular electronics, spintronics, or sensor applications [13–15]. In this context, the determination of the atomic structure of these Si NRs is of prime importance.

The first structural models were based on the assumption that the underlying Ag(110) surface was not structurally modified, except for the relaxation of the first atomic layers. Thus, several models were proposed that were essentially based on density functional theory (DFT) and comparison with scanning tunneling microscopy (STM) images where the Si NRs appear as composed of two (SNRs) or four (DNRs) rows of protrusions attributed to Si atoms [16–20]. A review of these models has recently been published, showing that most of them are in favor of a Si honeycomb structure that is eventually buckled [21]. Indeed, in some rare cases, a honeycomb pattern was observed in high-resolution STM images [8,22]. Based on these observations and the first dimer-based models proposed by He [16], a ball-and-stick model of DNRs composed of a double row of bonded Si hexagons was proposed [22]. However, Colonna *et al.* brought experimental evidence that such honeycomb-like structure should result from STM tip artifacts [8]. Moreover, the features observed by ARPES and attributed to a Dirac cone were shown to be related to folded Ag bands induced by the Si overlayer [23], and the optical reflectance signal from Si ultrathin film grown on Ag(110) was not compatible with the one expected for silicene [24].

In 2013, using STM and grazing incidence x-ray diffraction (GIXD), Bernard *et al.* provided compelling evidence of a Ag(110) surface reconstruction associated with the release of Ag atoms induced by the Si NR growth [7] and proposed a model for the underlying Ag(110) substrate having two of five missing Ag rows along $[1\bar{1}0]$. Although

GIXD is a powerful technique for the discrimination of superstructure models and for the refinement of atomic positions [5], there is no direct way to recover the atomic structure from the signal *ab initio*, in particular for the case of a substrate reconstruction. Nonetheless, two relevant models have recently been proposed on the basis of DFT calculations. The first model was proposed by Hogan *et al.* [25]. Among the various atomistic configurations explored, a model with a double zigzag chain of Si adatoms backbonded to Si dimers lying within the Ag missing rows was found to be the most stable missing-row model. The number of 8 Si atoms per (5×2) unit cell also corresponds to the coverage of 7×10^{14} at $/\mathrm{cm}^2$, which was experimentally determined for completion of the first Si layer in two different experimental works [7,25]. Very recently, a "pentasilicene" model with a higher coverage of 12 Si atoms per (5×2) unit cell has been proposed [26]. In this model, Si atoms are arranged into chains composed of pentagonal rings running along the missing rows with alternate orientation. This model, hereafter called "pentamer" model, has a coverage of 12 Si atoms per 5×2 unit cell, higher than the experimental value ($\approx 8 \pm 2$ Si atoms per 5×2 unit cell) reported in the experimental works [7,25], but is supported by XPS experiments indicating the presence of two different types of Si atoms with a ratio of 2:1 in concentration. Both the pentamer and zigzag models have been shown to present a good match with STM experiments; XPS alone is clearly not able to discriminate between these models.

This Letter is focused on the determination of the atomic structure of the Si NRs grown on Ag(110) using a study of combined GIXD, STM, and DFT. Among the numerous models reported in the literature, we will consider the most stable ones and/or those that integrate the missing-row reconstruction of Ag(110). We show that the Si DNRs correspond to twin Si pentamer chains with alternate orientations grown on the missing-row reconstructed surface: the atomistic configuration reported in [26] and refined with DFT calculations perfectly fits the experimental structure factors obtained by GIXD and is in strong agreement with STM observations. Apart from the debate regarding the silicene character of the Si NRs grown on Ag(110), we stress that our study definitively resolves the atomic structure of the Si DNRs arranged in a $(5 \times 2)/c(10 \times 2)$ superstructure that compose the ultrathin Si film grown on Ag(110) and, consequently, that of Si SNRs.

Experiments were performed *in situ* in ultrahigh vacuum (UHV) chambers (base pressure $<10^{-10}$ mbar). Sample cleaning was achieved by repeated cycles of Ar^+ sputtering and annealing at 873 K. Si was evaporated at a rate of $\sim$1 monolayer (ML)/h from a Si wafer piece heated by direct current and deposited on the Ag substrate maintained at 460 K [1 ML corresponds to the saturation coverage of the (5×2) or $c(10 \times 2)$ structure]. The STM observations were carried out at the CINaM in Marseille using STM Scienta Omicron systems, working at $T = 77$ K in constant-current mode. GIXD experiments were carried out at the ID3 beam line of the European Synchrotron Radiation Facility, using 17-keV x rays at an incidence angle of 0.22°. The basis is defined by $\vec{a}_x = a(0, 0, 1)$, $\vec{a}_y = a(½, -½, 0)$, $\vec{a}_z = a(½, ½, 0)$, where $a = 0.4085$ nm. The corresponding h, k, and l indices are used for indexing a reflection in reciprocal space.

Structure and total energy calculations were performed within local-density approximation using a plane-wave or norm-conserving pseudopotential framework [27] using 9- and 13-layer-thick slabs separated by vacuum. Results were compared with generalized gradient approximation (Perdew, Burke, and Ernzerhof [28]) calculations including semiempirical van der Waals corrections [29]. Structural relaxations using (2×5) and $c(2\times10)$ unit cells were performed at a kinetic energy cutoff of 30 Ry and a $(2\times8\times1)$ k-point mesh. Constant-height STM images were simulated using the Tersoff-Hamann approach [30]. Surface formation energies were computed using a standard thermodynamic expression $\gamma = [E_{\mathrm{slab}}(N_{\mathrm{Si}}, N_{\mathrm{Ag}}) - N_{\mathrm{Ag}}\mu_{\mathrm{Ag}}^{\mathrm{bulk}} - N_{\mathrm{Si}}\mu_{\mathrm{Si}}^{\mathrm{bulk}} - N_{\mathrm{Si}}(\mu_{\mathrm{Si}} - \mu_{\mathrm{Si}}^{\mathrm{bulk}})]/2A$ where $E_{\mathrm{slab}}(N_{\mathrm{Si}}, N_{\mathrm{Ag}})$ is the total energy of the (symmetric) slab of surface area A containing N_{Si} (N_{Ag}) atoms of Si (Ag), and μ is the appropriate chemical potential. Further details are given in [25].

Figure 1 shows calculated structural models and simulated STM images for various reconstruction models. These include the best missing-row-based models proposed in [25] (here termed zigzag A and B) and the pentamer model

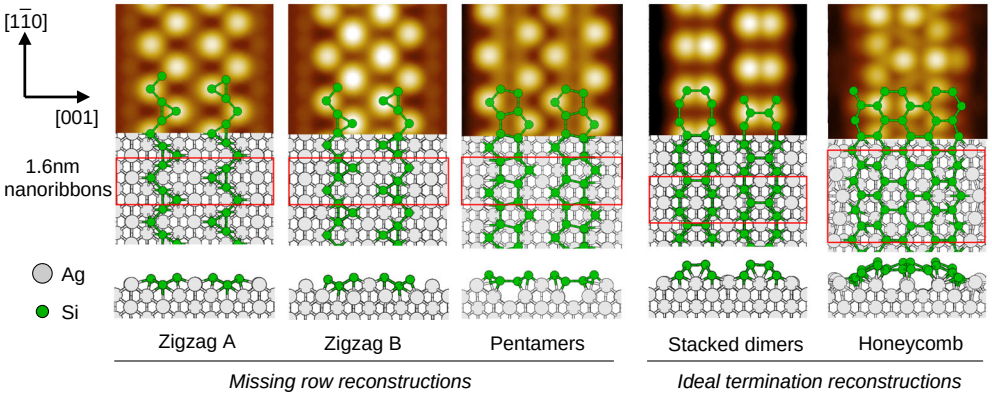

FIG. 1. Schematic models of 1.6-nm-wide Ag(110)-Si nanoribbons and their simulated STM images.

[26]. Other missing-row reconstructions, based on stacked dimers or honeycomb strips, were considered but found to be unstable, and are thus not shown here. For comparison, we have also included the most stable configurations found on nonreconstructed Ag surfaces, among the various models proposed in the literature [16–19,22]. These are the He $g1$ (here, "stacked dimers") model [16] and a zigzag-edge honeycomb (here, "honeycomb") model [18,25]. The complete theoretical comparison of the different honeycomb models can be found in [25]. We have not considered models [20] with Si coverage far above the value experimentally determined. No significant variations were found between the different approximations. Formation energies of each model are compared in Fig. 2 as a function of the deviation of the Si chemical potential from its bulk value. In the Si-poor part of the diagram, all structures are unstable with respect to the bare surface; experimentally, the surface exhibits small Si clusters and few NRs [8,26]. When $\mu_{\mathrm{Si}} - \mu_{\mathrm{Si}}^{\mathrm{bulk}} \geq -0.02$ eV, the pentamer chain phase becomes stable, corresponding to the formation of the large (5×2) or $c(10 \times 2)$-ordered domains observed by STM and GIXD [7,8] at 460 K. The honeycomb structure is favored only for large μ_{Si} values; it is never observed, however, because a second Si layer, having a $c(8 \times 4)$ structure [8], forms instead. This is in good agreement with the observation of a single Si phase during submonolayer growth [7,8,25]. Our new calculations thus demonstrate that the pentamer model is not only more stable than the zigzag models as stated by Cerda *et al.*, but also more stable than the high-coverage stacked-dimer and honeycomb models previously thought to be minimum energy structures [25].

As already widely reported in STM experiments, Si NRs are imaged as two or four rows of protrusions running along the $[1\bar{1}0]$ substrate direction for SNRs and DNRs, respectively (see Fig. S2 [31]). Figure 3 displays a high-resolution STM image of the Ag(110) surface partially covered with Si DNRs locally self-assembled in a (5×2) or $c(10 \times 2)$ superstructure. The honeycomb model can be rejected since it displays a $\times 4$ periodicity along $[1\bar{1}0]$, instead of the $\times 2$ periodicity widely experimentally reported. The stacked-dimers model, though having the correct periodicity, does not correspond to the experimental observations. The visualization of *both* the rectangular cell of the Ag(110) substrate and the protrusions of the DNRs on the same scan lines allows us to assess the different theoretical models to a finer precision than has been done previously [25,26]. In agreement with the simulated STM images shown in Fig. 1, only two models are found to match accurately the STM images, namely, the pentamer model [26] and the zigzag B model [25]. Both of them include the missing-row surface reconstruction proposed by Bernard *et al.* [7]. It has to be underlined that the atomic resolution obtained in the x and y directions allows us to unambiguously discriminate between the zigzag A and B models in favor of the latter one, which is, however, clearly energetically unfavored (Fig. 2). In STM images, the observed protrusions would mainly result from the proximity of the higher Si adatoms involved in the DNRs, in agreement with the fact that there is no contribution to the STM image from the Si atoms lying in the missing rows [25,26].

The pentamer model is the only model to be in agreement with both DFT and STM results. We now show that GIXD offers a strong independent confirmation of the atomic structure. As already mentioned [7], as soon as the Si evaporation starts at 460 K, ordered domains of Si DNRs with a (5×2) or $c(10 \times 2)$ reconstruction form, leading to the appearance of diffracted intensity for noninteger values of h. Typical scans are presented in Fig. S3 [31]. The diffraction peaks associated with the $5\vec{a}_x$ periodicity are very narrow, with a FWHM of 0.033 and 0.003 along the h and k

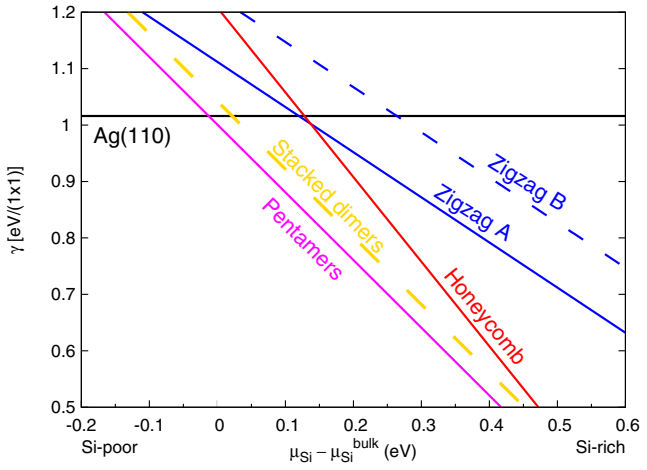

FIG. 2. Computed DFT-LDA formation energies for the structural models shown in Fig. 1, plotted with respect to the deviation of the Si chemical potential from its bulk value. Corresponding results using generalized gradient approximation-van der Waals are shown in Fig. S1 [31].

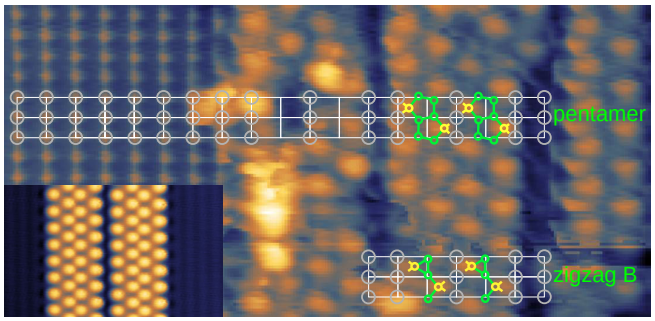

FIG. 3. STM image (9×4.5 nm^2) of Si DNRs below 1 ML. The high resolution allows us to visualize both the Ag atoms (left part) of the (110) substrate and the protrusion of the DNRs (right part). Both pentamer and zigzag B models match the STM image. Si adatoms (yellow circles) appear as protrusions in the STM images whereas Si atoms in the missing rows (green circles) are not imaged. $I = 50$ nA, $V_{\mathrm{sample}} = 100$ mV. The high tunneling current used to resolve the atomic structure of the Ag(110) substrate induced a partial alteration of the Si nanoribbons. The inset in the bottom-left corner shows two unaltered Si DNRs imaged at a lower tunneling current [($7.5 \times 4.5\,\mathrm{nm}^2$), $I = 480$ pA, $V_{\mathrm{sample}} = 40$ mV]. See also Fig. S2(b) [31].

directions, respectively, and corresponding to domains spreading on the whole terraces along the y direction, with a mean domain size of $\sim$12 nm in the x direction, in agreement with STM observations. In contrast, for fractional k values ($k = n + 1/2$), there is no significant signal associated with the doubling of the unit cell along y. This is due to the simultaneous formation of very small (5×2) and $c(10 \times 2)$ domains, leading to a very large width for the corresponding satellite rods at fractional k values, which can thus practically not be distinguished from the background. We have measured 44 in-plane structure factors, corresponding to a set of 17 nonequivalent reflections, and 292 out-of-plane structure factors along 11 nonequivalent rods. Details of measurements, correction factors [32], and uncertainty estimation are given in the Supplemental Material [31].

We have compared the experimental results with the various models discussed previously. For this purpose, we have assumed a noncoherent mixing of (5×2) and $c(10\times2)$ domains. As free parameters, we have used two scale factors (for crystal truncation rods and superstructure rods, respectively), and Debye-Waller factors for Si and Ag surface atoms. The agreement between experimental (F_{exp}) and simulated (F_{th}) structure factors is estimated by the value of $\chi^2 = [1/(N_{\mathrm{pt}} - N_{\mathrm{par}})]\sum^{N_{\mathrm{pt}}}[(F_{\mathrm{th}} - F_{\mathrm{exp}})/\sigma_{\mathrm{exp}}]^2$, where N_{pt} is the number of experimental structure factors and N_{par} is the number of free parameters.

Obviously, models that do not take into account the missing-row reconstruction of the surface do not give a good agreement with the diffraction experiments. $\chi^2 \approx 41$ is found for the stacked-dimer model (see Fig. S4 for a comparison of experimental and theoretical structure factors [31]), and $\chi^2 \approx 38$ is found for the honeycomb model. In contrast, the recent models proposed based on a surface where two out of five Ag rows are missing should give a better agreement. Whereas both zigzag A and zigzag B models give a poor agreement, with $\chi^2 \approx 33$ and $\chi^2 \approx 32$, respectively, a good fit is obtained with the pentamer model, with $\chi^2 \approx 13$. To illustrate the fit quality, we compare the experimental and theoretical structure factors derived from the zigzag B and pentamer models in Fig. 4.

In order to go further, we have studied the robustness of the pentamer model by allowing the atomic positions to relax from their equilibrium position, using simulated annealing and Levenberg-Marquardt fitting procedures. We have used as additional free parameters the relaxations of the Si atoms and the Ag atoms for the added rows and for the first complete plane. Moreover, we have not taken into account the Si and surface Ag relaxations along y because, due to the absence of measurable rods for fractional values of k, we are not sensitive to them. Because of the symmetry of the unit cell, the number of free parameters for Ag relaxations is 13 and that for Si relaxations is 8. The Ag relaxations propagate elastically into the substrate. As the crystal is highly anisotropic, the attenuation length of the elastic relaxations is larger than expected for an isotropic substrate [33]. We have numerically computed the elastic relaxations for the next 20 Ag layers, using a semiempirical potential based on the tight-binding approximation [34] and well adapted for the

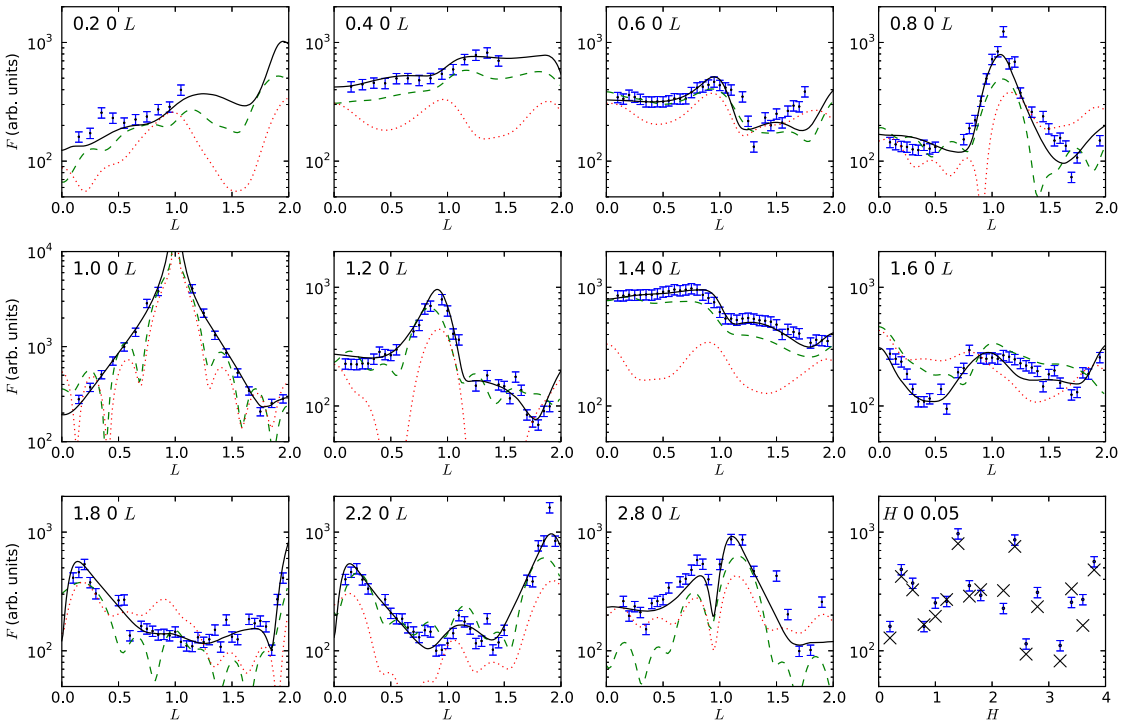

FIG. 4. Comparison between experimental (blue dots) and simulated structure factors along various rods, and for in-plane structure factors. Red dotted line: raw DFT results (PBE, 13-layer thick slabs) for the zigzag B model. Green dashed line: raw DFT results for the pentamer model. Black continuous line and black crosses: after refinement of the atomic positions for the pentamer model.

description of the relaxations of transition metal surfaces [35]. The fit shows that the pentamer model is stable and, with additional small relaxations, the fit converges to a value $\chi^2 \approx 3.4$. The comparison drawn in Fig. 4 (black continuous line) shows that the agreement is very good for all rods. In particular, the high intensity of the (1.4 0 L) rod is very well reproduced. The Si and Ag atomic positions in the unit cell are given in Table S1 and sketched in Fig. S5 [31].

In conclusion, we present in this Letter a combined experimental and theoretical study which definitively attests to the pentamer chain structure of the Si NRs grown on Ag(110). We have screened all proposed nanoribbon models according to three independent criteria: STM imaging, DFT formation energies, and GIXD experiments (the results are summarized in Table S2 [31]). While two models are found to perfectly match STM experiments, only the pentamer model is also energetically stable under typical experimental conditions and reproduces well the GIXD experiments. We stress that this important finding will help to understand the interesting electronic properties of Si nanoribbons, in comparison with those of silicene. Our result also reinforces interest in studying the adsorption properties of a wide range of species in the framework of realizing future nanometric devices that use these building blocks compatible with conventional Si-based electronics.

Support from the ID3 beamline staff at ESRF is greatly acknowledged. C. H. acknowledges the CINECA award under the ISCRA initiative for the availability of high-performance computing resources and support. We thank Fabio Ronci and Yves Borensztein for fruitful discussions.

*Corresponding author.
prevot@insp.jussieu.fr
†Corresponding author.
masson@cinam.univ-mrs.fr
‡Present address: Department of Energy Science (DOES), Sungkyunkwan University, N Center, Jangan-gu, Gyeonggi-do, Suwon 16419, South Korea.

[1] G. Guzmán-Verri and L. Lew Yan Voon, Phys. Rev. B **76**, 075131 (2007).
[2] S. Cahangirov, M. Topsakal, E. Aktürk, H. Şahin, and S. Ciraci, Phys. Rev. Lett. **102**, 236804 (2009).
[3] C. Grazianetti, E. Cinquanta, and A. Molle, 2D Mater. **3**, 012001 (2016).
[4] P. Vogt, P. De Padova, C. Quaresima, J. Avila, E. Frantzeskakis, M. C. Asensio, A. Resta, B. Ealet, and G. Le Lay, Phys. Rev. Lett. **108**, 155501 (2012).
[5] A. Curcella, R. Bernard, Y. Borensztein, A. Resta, M. Lazzeri, and G. Prévot, Phys. Rev. B **94**, 165438 (2016).
[6] C. Leandri, G. L. Lay, B. Aufray, C. Girardeaux, J. Avila, M. E. Dávila, M. C. Asensio, C. Ottaviani, and A. Cricenti, Surf. Sci. **574**, L9 (2005).
[7] R. Bernard, T. Leoni, A. Wilson, T. Lelaidier, H. Sahaf, E. Moyen, L. Assaud, L. Santinacci, F. Leroy, F. Cheynis, A. Ranguis, H. Jamgotchian, C. Becker, Y. Borensztein, M. Hanbücken, G. Prévot, and L. Masson, Phys. Rev. B **88**, 121411(R) (2013).
[8] S. Colonna, G. Serrano, P. Gori, A. Cricenti, and F. Ronci, J. Phys. Condens. Matter **25**, 315301 (2013).
[9] P. De Padova, C. Quaresima, C. Ottaviani, P. M. Sheverdyaeva, P. Moras, C. Carbone, D. Topwal, B. Olivieri, A. Kara, H. Oughaddou, B. Aufray, and G. Le Lay, Appl. Phys. Lett. **96**, 261905 (2010).
[10] L. Michez, K. Chen, F. Cheynis, F. Leroy, A. Ranguis, H. Jamgotchian, M. Hanbücken, and L. Masson, Beilstein J. Nanotechnol. **6**, 777 (2015).
[11] P. De Padova, C. Quaresima, B. Olivieri, P. Perfetti, and G. Le Lay, J. Phys. D **44**, 312001 (2011).
[12] H. Sahaf, L. Masson, C. Léandri, B. Aufray, G. Le Lay, and F. Ronci, Appl. Phys. Lett. **90**, 263110 (2007).
[13] E. Salomon and A. Kahn, Surf. Sci. **602**, L79 (2008).
[14] E. Salomon, T. Angot, C. Thomas, J.-M. Layet, P. Palmgren, C. I. Nlebedim, and M. Göthelid, Surf. Sci. **603**, 3350 (2009).
[15] E. Salomon and T. Angot, Sci. Technol. Adv. Mater. **3**, 354 (2011).
[16] G. He, Phys. Rev. B **73**, 035311 (2006).
[17] A. Kara, S. Vizzini, C. Leandri, B. Ealet, H. Oughaddou, B. Aufray, and G. LeLay, J. Phys. Condens. Matter **22**, 045004 (2010).
[18] C. Lian and J. Ni, Physica (Amsterdam) **407B**, 4695 (2012).
[19] M. R. Tchalala, H. Enriquez, A. J. Mayne, A. Kara, G. Dujardin, M. A. Ali, and H. Oughaddou, J. Phys. Conf. Ser. **491**, 012002 (2014).
[20] B. Feng, H. Li, S. Meng, L. Chen, and K. Wu, Surf. Sci. **645**, 74 (2016).
[21] B. Aufray, B. Ealet, H. Jamgotchian, H. Maradj, J.-Y. Hoarau, and J.-P. Biberian, in *Silicene: Structures, Properties and Applications*, edited by M. J. S. Spencer and T. Morishita (Springer International Publishing, Cham, 2016), p. 183.
[22] H. Sahaf, C. Léandri, E. Moyen, M. Macé, L. Masson, and M. Hanbücken, Europhys. Lett. **86**, 28006 (2009).
[23] P. Gori, O. Pulci, F. Ronci, S. Colonna, and F. Bechstedt, J. Appl. Phys. **114**, 113710 (2013).
[24] Y. Borensztein, G. Prévot, and L. Masson, Phys. Rev. B **89**, 245410 (2014).
[25] C. Hogan, S. Colonna, R. Flammini, A. Cricenti, and F. Ronci, Phys. Rev. B **92**, 115439 (2015).
[26] J. I. Cerdá, J. Sławińska, G. Le Lay, A. C. Marele, J. M. Gómez-Rodríguez, and M. E. Dávila, Nat. Commun. **7**, 13076 (2016).
[27] P. Giannozzi *et al.*, J. Phys. Condens. Matter **21**, 395502 (2009).
[28] J. P. Perdew and A. Zunger, Phys. Rev. B **23**, 5048 (1981).
[29] S. Grimme, J. Comput. Chem. **27**, 1787 (2006).
[30] J. Tersoff and D. R. Hamann, Phys. Rev. B **31**, 805 (1985).
[31] See Supplemental Material at http://link.aps.org/supplemental/10.1103/PhysRevLett.117.276102, which includes GGA-vdW calculations, STM images, GIXD scans, the comparison between experimental and theoretical structure factors derived from the stacked-dimers model, and the atomic configuration of the Si pentamers corresponding to the best fit of the GIXD experiments.
[32] O. Robach, Y. Garreau, K. Aïd, and M. B. Véron-Jolliot, J. Appl. Crystallogr. **33**, 1006 (2000).
[33] B. Croset and G. Prévot, Phys. Rev. B **73**, 045434 (2006).
[34] V. Rosato, M. Guillope, and B. Legrand, Philos. Mag. A **59**, 321 (1989).
[35] G. Prevot, C. Cohen, D. Schmaus, P. Hecquet, and B. Salanon, Surf. Sci. **506**, 272 (2002).